SASEC2015
Third Southern African Solar Energy Conference
11 – 13 May 2015
Kruger National Park, South Africa

LAMINAR FLOW HEAT TRANSFER FOR ASYMMETRICAL NON-UNIFORM HEAT FLUX DISTRIBUTIONS ON HORIZONTAL CIRCULAR TUBES

Izuchukwu F. Okafor, Jaco Dirker* and Josua P. Meyer
*Author for correspondence
Department of Mechanical and Aeronautical Engineering,
University of Pretoria, Pretoria, South Africa
*e-mail: jaco.dirker@up.ac.za

ABSTRACT

In this study, the influence of symmetrical and asymmetrical non-uniform heat flux distribution boundaries in terms of the gravitational field on the internal heat transfer coefficient and the friction factor in a horizontal circular tube was investigated numerically. Of interest was buoyancy driven flow in the laminar flow regime. Inlet fluid temperature and external loss convective heat transfer was also considered. Three-dimensional steady-state numerical simulations were performed using ANSYS Fluent version 14. Circumferential non-uniform heat flux was simulated as a sinusoidal function of the heat flux incident on the tube. A steel tube was considered which had a wall thickness of 5.2 mm, a length-to-inner-diameter ratio of 160, and a thermal conductivity of 16.27 W/mK. The results showed that the average internal heat transfer coefficients and friction factors for the symmetrical non-uniform heat flux distribution cases were higher than that of the asymmetrical case considered. The heat transfer coefficient also increased with an increase in the inlet fluid temperature for the uniform heat flux, symmetrical and asymmetrical non-uniform heat flux distributions cases. However, the average internal heat transfer coefficient decreased with the increase in the external loss convective heat transfer coefficient. It was found that the friction factor decreased with increase in the fluid inlet temperature and external loss convective heat transfer coefficient for the uniform heat flux, symmetrical and asymmetrical non-uniform heat flux distributions cases.

Keywords: uniform and non-uniform heat flux, heat transfer coefficients, friction factor, buoyancy driven flow

INTRODUCTION

Heat transfer in circular tubes is essential in many engineering applications such as heat exchangers, solar thermal collectors and boilers etc. In these systems, the exterior walls of the tubes are usually subjected to either circumferential uniform or non-uniform heat flux boundary conditions. Extensive experimental and numerical studies have been conducted for the case of circumferential uniform heat flux boundary conditions [1-5]. Studies are still lacking for the case of non-uniform heat flux boundary conditions, which could be due to the complexity of such thermal boundary conditions. Zeitoun [6] numerically investigated the heat transfer for laminar flow in partial uniformly heated horizontal tubes, without considering buoyancy effects. In a previous study [7] conducted by the present authors, non-uniform heat flux distributions boundary case were considered and it was found that the heat transfer characteristics of horizontal circular tubes subjected to circumferential non-uniform heat flux symmetrical with the heat flux boundary for laminar flow were quite different from that of uniform heat flux boundary condition. This was attributed to buoyancy effects resulting from the temperature differential over the circumferential wall surface of the tube. The prior study was, however, only conducted for conditions where the heat flux distribution was symmetrical in terms of the gravitational field direction. The present study investigates both symmetrical cases (with gravity directed at $\gamma = 0°$) as well as asymmetrical cases (with gravity directed at $\gamma = 30°$) in a horizontal circular tube.

NOMENCLATURE

A	[m^2]	surface or cross sectional area
f	[-]	Darcy friction factor
g	[m/s^2]	acceleration due to gravity
$h, \bar{h}$	[W/m^2K]	heat transfer coefficient and average heat transfer coefficient
I	[-]	number of heated divisions
i	[-]	heated division number
k	[W/m K]	thermal conductivity
L, L_{TOT}	[m]	axial dimension and total axial length of tube
M	[-]	total number of the axial divisions
(m, n)	[-]	numerical surface location
N	[-]	total number of the circumferential divisions
Nu $\overline{\text{Nu}}$	[-]	Nusselt number and average Nusselt number
q	[W]	heat transfer
q''	[W/m^2]	heat flux
R , $\bar{R}$	[m]	radius and average radius
r	[m]	radial coordinate
$T, \bar{T}$	[K]	temperature and average temperature
t	[m]	tube wall thickness
v	[m/s]	velocity
x	[m]	axial coordinate
Greek Letters		
α	[°]	angle span of the heated segment of the tube
β	[K^{-1}]	thermal expansion coefficient of heat transfer fluid
γ	[°]	gravity inclination with heat flux boundary
ε_{tu}	[-]	emissivity of the tube-wall surface
ρ	[kg/m^3]	density of the heat transfer fluid
σ_{SB}	[W/m^2K^4]	Stefan-Boltzmann constant
ϕ	[°]	angle span of each circumferential division or tangential dimension
Subscript		
a , atm		free stream air , atmosphere
∞		radiant surroundings
b		bulk fluid property
$conv$		convection
f , i		fluid , inner surface
m, n		at position m, n
o		outer surface
r , rad		in radial direction , radiation
tu ,w		tube , wall

PHYSICAL MODEL AND PROBLEM DESCRIPTION

Figure 1 shows the geometry of the tube model being considered, with the gravity at an angle of γ. The tube had an outer radius of R_o = 73 mm an inner radius of 62.7 mm (based on a wall thickness of t = 5.2 mm), a length to inner-diameter ratio of approximately 160 and a thermal conductivity of 16.27 W/mK. The tube was divided into $M \times N$ number of sections in the axial and circumferential directions. Figure 2 gives a representation of the cross-section of the tube model in Figure 1, under the influence of the gravity body force (g) at an angle of γ with respect to the heat flux boundary. It shows the numbering system for simulating the heat flux distributions around the tube.

The non-uniform heat flux distribution (indicated by shading) which covers a radiated angle of α was modeled based on sinusoidal function of the heat flux distributions employed in our earlier study on the turbulent flow case [8], which noted that the heat flux distributions on a tube in a horizontal orientation heated from the bottom was non-uniform as in the case of the absorber tube receiver of a linear Fresnel solar collector.

Also, the deviation of the non-uniform heat flux distribution boundary (gravity at γ > 0°) from the symmetrical axis of the tube model could occur when the irradiation from the sun was not at the zenith angle position and this could influence the heat transfer characteristics of the tube. The temperature differential along the circumferential wall of the tube due to non-uniform heat flux distributions could create density variations within the fluid. This could influence the forced convection heat transfer processes in the tube due to the buoyancy-induced secondary flow resulting from the density variations within the fluid.

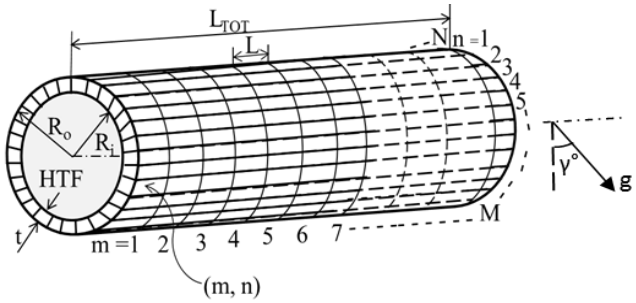

Figure 1 Geometry of the tube model.

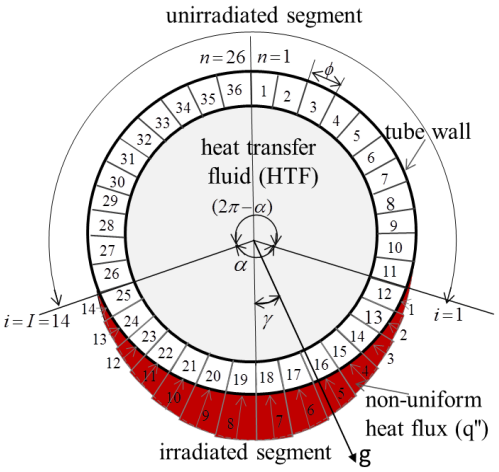

Figure 2 Cross-section of the tube model in Figure 1

The temperature dependent density of the heat transfer fluid was modelled based on the Boussinesq approximation [9] expressed in Eqn. (1).

$$\rho = \rho_o(1-\beta\Delta T) \tag{1}$$

where is the ρ_o constant density, ΔT is the temperature change and β is the thermal expansion coefficient of the heat transfer fluid.

NUMERICAL FORMULATION AND HEAT TRANSFER MODEL

The circumferential wall of the tube model was divided into N = 36 segments as shown in Figure 2 and each of the segments subtend an angle span of ϕ defined as:

$$\phi = \frac{2\pi}{N} \tag{2}$$

The segment, $n_{i=1}$ (in a clockwise fashion) represents where the heat flux distribution starts and can be expressed in terms of α in Eqn. (3).

$$n_{i=1} = \frac{\left[N-(\alpha/2\pi)\times N\right]}{2}+1 \tag{3}$$

where n = *1, 2, 3… N = 36, and* i = *1, 2, 3… I.* I is the number of segments of the tube model which directly received the heat flux expressed in eqn. (3) and α is in the multiple of 20°.

$$I = \frac{\alpha}{2\pi}N \tag{4}$$

The heat transfer model under steady-state condition can be obtained, by applying the energy balance principle on the element at (n, m) shown in Figure 1, expressed as follows:

$$q_{o,(m,n)} = q_{i,(m,n)} + q_{x,(m,n)} + q_{x,(m+1,n)} + q_{\phi,(m,n)} + q_{\phi,(m,n+1)} + q_{o,conv,(m,n)} + q_{o,rad,(m,n)} \tag{5}$$

Where $q_{o,(m,n)}$ is the heat transfer rate on the outer wall surface at location (m, n) given in Eqn. (6) as follows:

$$q_{o,(m,n)} = q''_{o,(m,n)}A_o \tag{6}$$

Also $q_{i,(m,n)}$ is the heat transfer rate to the working fluid at location (m, n) which can be expressed as follows:

$$q_{i,(m,n)} = h_{i,(m,n)}.A_{i,(m,n)}(T_{wi,(m,n)} - T_{b,m}) \tag{7}$$

where $h_{i,(m,n)}$ is the local internal heat transfer coefficient, $A_{i,(m,n)}$ is the inner wall surface area, $T_{wi,(m,n)}$ is the inner wall temperature and $T_{b,m}$ is the fluid bulk temperature. The average circumferential internal heat transfer coefficient at position m, $\bar{h}_{i,m}$, can be used to express the average Nusselt number at position m as follows:

$$\overline{Nu}_{i,m} = \frac{\bar{h}_{i,m}2R_i}{k_f} \tag{8}$$

The average circumferential internal heat transfer coefficient can be expressed as:

$$\bar{h}_{i,m} = \frac{\sum_{n=1}^{N} q_{i,(m,n)}}{2\pi R_i L\left(\bar{T}_{w,i,m} - T_{b,m}\right)} \quad (9)$$

Here $\bar{T}_{w,i,m}$ is the circumferential average local inner-wall temperature.

In eqn. (5) $q_{o,conv,(m,n)}$ is the forced convective heat transfer loss from the outer-wall surface at (m, n) to the surroundings modeled from Newton's law of cooling [9]as:

$$q_{o,conv,(m,n)} = h_{o,(m,n)} A_o (T_{w,o,(m,n)} - T_a) \quad (10)$$

Here $T_{w,o,(m,n)}$ is the outer-wall temperature at (m,n) and T_a is the ambient free stream air temperature. $h_{o(m,n)}$ is the external loss convective heat transfer coefficient [10] related to the wind velocity, v_a *(m/s)* around the tube model is expressed in Eqn. (11) as:

$$h_{o(m,n)} = \bar{h}_o = 5.7 + 3.8v \quad (11)$$

Also in eqn. (5), $q_{o,rad,(m,n)}$ is the radiative heat transfer loss to the surroundings modelled from the Stefan-Boltzmann law of the emissive power of a surface at a thermodynamic temperature as follows:

$$q_{o,rad,(m,n)} = \varepsilon_{tu} \sigma_{SB} A_o (T^4_{w,o,(m,n)} - T^4_{\infty}) \quad (12)$$

Here ε_{tu} is emissivity of the tube model expressed in terms of the tube outer-wall temperature as follows: $\varepsilon_{tu} = 0.0003 T_{w,o,(m,n)} + 0.3171$ [11] and σ_{SB} is the Stefan-Boltzmann constant (5.67×10^{-8} W/m^2. K^4)[9]. T_∞ is the temperature of the surrounding.

In Eqn. (5), $q_{\phi,(m,n)}$ and $q_{\phi,(m,n+1)}$ are the conductive heat transfers in the tangential direction modelled with the Fourier law of heat conduction [9]. Also, $q_{x,(m,n)}$ and $q_{x,(m+1,n)}$ are the conductive heat transfers in the axial direction modelled from Fourier's law of heat conduction.

The $\bar{h}_{i,m}$ and $\bar{T}_{w,i,m}$ in Eqn. (9) are determined by performing numerical simulations for steady-state and laminar flow implemented in ANSYS Fluent version 14.0 [12] for uniform heat flux distributions, symmetrical (gravity at γ = 0°) and asymmetrical (gravity at γ = 30°) non-uniform heat flux distributions with the heat flux boundary.

FLUID FLOW THROUGH THE TUBE MODEL

The fluid flow through the tube model in Figure 1 was assumed incompressible, steady-state and laminar. Also, the fluid flow through the tube encounters pressure drop due to friction loss at the internal wall boundary of the tube. The pressure drop (Δp) along the tube length (L_{TOT}) is expressed as [9]:

$$\Delta P = f \frac{L_{TOT}}{2R_i} \frac{\rho V^2_{ave.}}{2} \quad (13)$$

Table 1 External surface heat transfer boundary conditions

Heat flux distribution	Heat transfer on external surface	Wall element range
Uniform:	$q_{w,(m,n)} = A_o q''$	$m \in [1, M]$ and $n \in [1, n_{i=1}) \cup [n_{i=1} + I, N]$
Non-uniform:		
Un-irradiated element:	$q_{w,(m,n)} = 0$	$m \in [1, M]$ and $n \notin [1, n_{i=1}) \cup [n_{i=1} + I, N]$
Irradiated element:	$q_{o,(m,n)} = A_o q''\left(\frac{\pi}{2}\right) \times \sin\left[\frac{\pi}{\alpha}\phi(n - n_{i=1} + \frac{1}{2})\right]$	$m \in [1, M]$ and $n \in [1, n_{i=1}) \cup [n_{i=1} + I, N]$

where V_{ave} is the mean fluid velocity and f is the friction factor.

The governing equations of the fluid flow and heat transfer in the tube model were the continuity, momentum and energy equations presented in vector form [13] given as follows:

Continuity: $\nabla \cdot \vec{V} = 0$ (14)

Momentum: $\rho(\vec{V} \cdot \nabla)\vec{V} = -\nabla p + \mu \nabla^2 \vec{V} + \rho \vec{g}$ (15)

Energy: $V \cdot (\vec{V}(\rho c_p T)) = \nabla \cdot (k \nabla T)$ (16)

where $\nabla \equiv \frac{1}{r}\frac{\partial}{\partial r} + \frac{1}{r}\frac{\partial}{\partial \phi} + \frac{\partial}{\partial x}$ and $\vec{V} = v_r + v_\theta + v_x$

BOUNDARY CONDITIONS

The following boundary conditions were applied:

(i) Inlet boundary conditions (x = 0):

$$\dot{m}_x(r, \phi) = \text{ uniform and } \dot{m}_r = \dot{m}_\phi = 0 \text{ kg/s} \quad (17)$$

$$T_f(r, \phi) = T_{b,o} = 300 \text{ K} \quad (18)$$

(ii) Outlet boundary condition ($x = L_{TOT}$):

$$P(r, \phi) = P_{atmp} \quad (19)$$

(iii) Tube inner wall surface boundary condition (r = R_i):

$$v_r = v_\phi = v_x = 0 \quad (20)$$

(iv) External wall surface boundary conditions ($r = R_o$):

The external wall surface boundary conditions used for the uniform and non-uniform heat flux distributions are given in Table 1. Two different heat flux intensities base levels, being q'' = 7.1 kW/m^2 and 14.7 kW/m^2 were considered in this study. The sinusoidal non-uniform heat flux distribution case was such that the lower central segments of the tube received the highest heat transfer rates. While, the heat transfer rates of the remaining irradiated element segments decreases to zero towards the un-irradiated upper portion of the tube.

NUMERICAL PROCEDURE AND MODEL VALIDATION

Eqns. (14) – (16) were solved numerically by the finite volume method described by Patankar [14]. The convective terms in the momentum and energy equations were discretised and solved using a second-order upwind scheme and the standard SIMPLEC algorithm was used for the

pressure-velocity coupling. A grid independence study was also conducted and it was ensured that the grid was sufficiently fine not to have a significant impact on the numerical results. The convergence criteria for the continuity, momentum and energy equations were set at minimum residual values of 10^{-6} and 10^{-8} respectively. The heat flux boundary conditions in Table 1 were implemented according to the angular position of the boundary cell via user defined functions. The physical properties of the tube model and heat transfer fluid used in the numerical study are presented in Table 2.

The model validation was conducted by comparing the numerical axial local Nusselt number with the analytical expression, $Nu_D = 4.36$ for a 360° span of uniform heat flux at inlet Reynolds number of 202, for fluid density independent of temperature. Figure 3 shows the results for the axial local Nusselt number for the numerical simulation of 360° span of uniform heat flux distribution with the intensity base level of 7.1 kW/m^2 compared with that of analytical expression. It shows that the axial local Nusselt number obtained from the numerical model was in good agreement with analytical expression.

RESULTS AND DISCUSSION

Heat transfer coefficient for uniform and non-uniform heat flux heat flux distributions

Figure 4 shows the variations of the average internal heat transfer coefficient for different inlet fluid temperature for α = 360° uniform and non-uniform heat flux distribution intensities base level of 7.1kw/m^2 and 14.2 kW/m^2 respectively. The non-uniform heat flux distribution was symmetrical with the vertical axis of the heat flux boundary

Table 2 Properties of the heat transfer fluid and tube model material.

Property	Heat transfer fluid (water)	Steel tube model
Density (ρ_o) [kg/m^3]	998.2	8030
Specific heat capacity [J/kgK]	4182	502.48
Thermal conductivity [W/mK]	0.61	16.27
Viscosity (μ) [N s/m^2]	0.001003	-
HTF temperature [K]	300	-

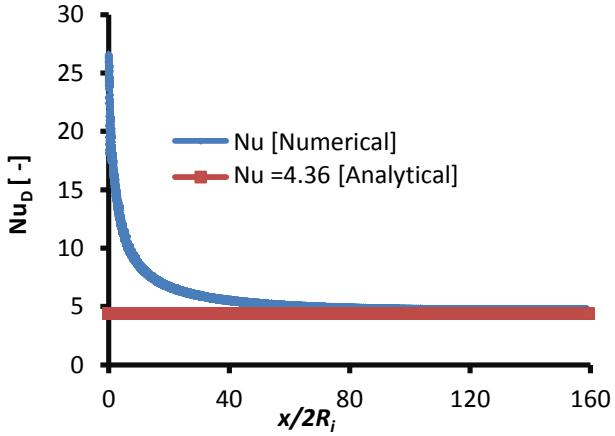

Figure 3 Axial local Nusselt number for numerical and analytical expression

of the tube model. It was found that the average internal heat transfer coefficient increased with the increase in the fluid inlet temperature. It was also found that the average internal heat transfer coefficient for the non-uniform heat flux case was higher than that of the uniform heat flux case. This was attributed to the influence of buoyancy effect resulting from the temperature differential over the circumferential tube wall. The average internal heat transfer coefficient for the non-uniform heat flux case of 14.2kW/m^2 was 13.2 % higher than that of uniform heat flux, while that of the non-uniform heat flux case of 7.1kw/m^2 was 12 % higher than that of uniform heat flux case.

Figure 5 shows the influence of the external loss convective heat transfer coefficient on the average internal heat transfer coefficient for α = 360° uniform and sinusoidal non-uniform heat flux distribution at the inlet Reynolds number of 800. For both cases, it was found that the average internal heat transfer coefficient decreased with the increase in the external loss convective heat transfer coefficient of the tube model. It was also found that the average internal heat transfer coefficient for the non-uniform heat flux case was as well higher than that of the uniform heat flux case.

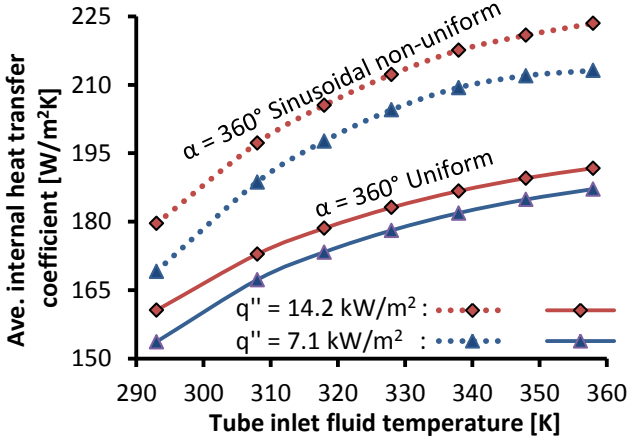

Figure 4 Variation of average internal heat transfer coefficient with the inlet fluid temperature

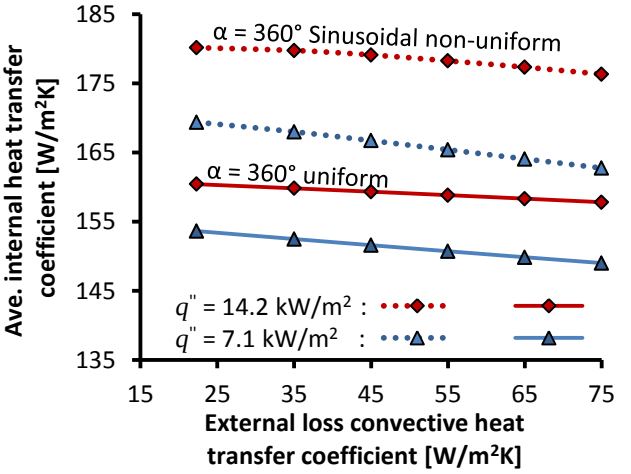

Figure 5 Influence of external loss convective heat transfer coefficient on internal heat transfer coefficient

Heat transfer coefficient for symmetrical and asymmetrical non-uniform heat flux distributions

Figure 6 shows the variations of the average internal heat transfer coefficient for different inlet fluid temperature where the sinusoidal non-uniform heat flux distributions were symmetrical ($\gamma = 0°$) and asymmetrical ($\gamma = 30°$) with the heat flux boundaries respectively. It was found that the average internal heat transfer coefficient decreased with the increase in γ and this could be due to the decrease in the buoyancy effect as γ was increased with respect to the heat flux boundary. This resulted in lower intensity secondary flow patterns (not included in this paper). The average internal heat transfer coefficient for the case of 14.2 kW/m^2, where $\gamma = 0°$ was 1.7 % higher than where $\gamma = 30°$ and similarly for the case of 7.1 kW/m^2 was 1.8 % higher where $\gamma = 0°$ than where $\gamma = 30°$ case. This revealed that the average internal heat transfer coefficient of the tube model considered was sensitive to the orientation of the heat flux distributions boundary.

Figure 7 shows the influence of the external loss convective heat transfer coefficient on the average internal heat transfer coefficient also where the sinusoidal non-uniform heat flux distributions were symmetrical ($\gamma = 0°$) and asymmetrical ($\gamma = 30°$) with the heat flux boundary. The average internal heat transfer coefficient decreased with the increase in the external loss convective heat transfer coefficient.

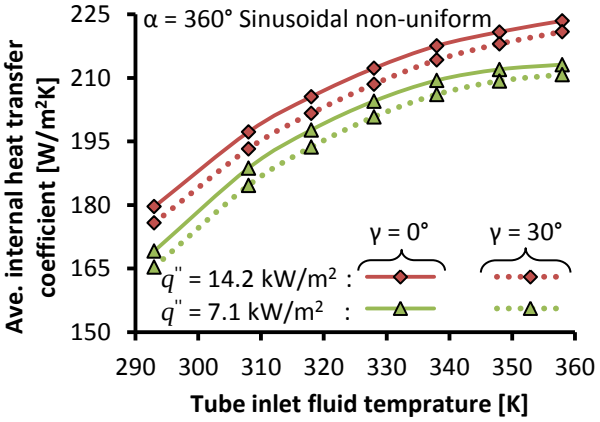

Figure 6 Variation of average internal heat transfer coefficient with fluid inlet temperature

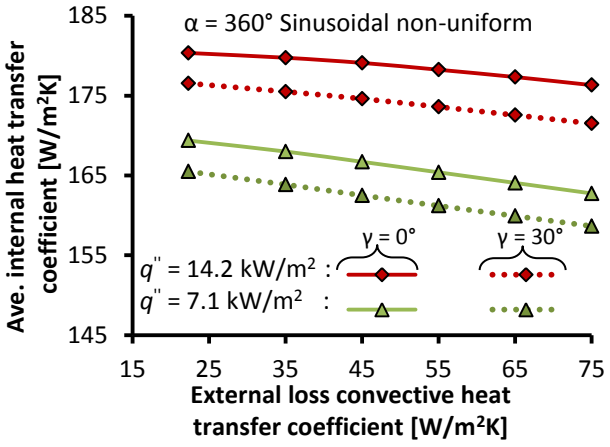

Figure 7 Influence of external loss convective heat transfer coefficient on internal heat transfer coefficient

It also decreased with the increase in γ as in the case of Figure 6, which could also be due to the decrease in the buoyancy effect with the increase in γ. The average internal heat transfer coefficient for the case of 14.2 kW/m^2 and 7.1 kW/m^2 where $\gamma = 0°$ was 2.5 % respectively higher than where $\gamma = 30°$. However, the effect of γ on the average internal heat transfer coefficient was found to be higher with the variation of the external loss convective coefficient than for the case of different inlet fluid temperature, indicating less influence of buoyancy effect with the increase in fluid inlet temperature.

Friction factor for uniform and non-uniform heat flux heat flux distributions

Figure 8 shows the variation of friction factor for different inlet fluid temperature for $\alpha = 360°$ uniform and non-uniform heat flux distribution intensities base level of 14.2 kW/m^2 and 7.1 kW/m^2 respectively. The non-uniform heat flux distribution cases are shown with the broken lines. It was found that the friction factor for the uniform and non-uniform cases decreased with the increase in the fluid inlet temperature and this could be due to decrease in the fluid density with the increase temperature. It was also found that the friction factor for the non-uniform heat flux case was higher than that of the uniform heat flux case. This was attributed to the higher influence buoyancy effect for the non-uniform heat flux case than that of the uniform heat flux case. The friction factor for the non-uniform heat intensity base level of 14.2 kW/m^2 was 10.4% higher than that of uniform heat flux case, while friction factor for non-uniform heat flux intensity base level of 7.1 kW/m^2 was 10.5% higher than that of uniform heat flux case.

Friction factor for symmetrical and asymmetrical non-uniform heat flux distributions

Figure 9 shows the variations of the friction factor for different inlet fluid temperature for the non-uniform heat flux distribution case in Figure 6. It was found that the friction factor for both the symmetrical ($\gamma = 0°$) and asymmetrical ($\gamma = 30°$) cases decreased with increase in the fluid inlet temperature. This was also attributed to the decrease in the fluid density with the increase temperature. It was also found that friction factor decreased with the increase in γ and this could be due to the influence of buoyancy-induced secondary flow.

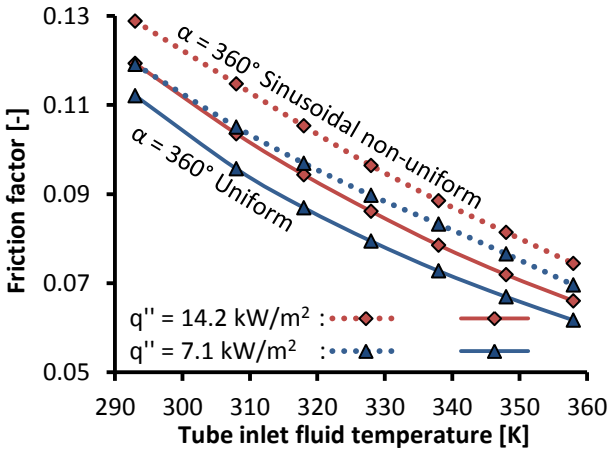

Figure 8 Variation friction factor with the fluid inlet temperature

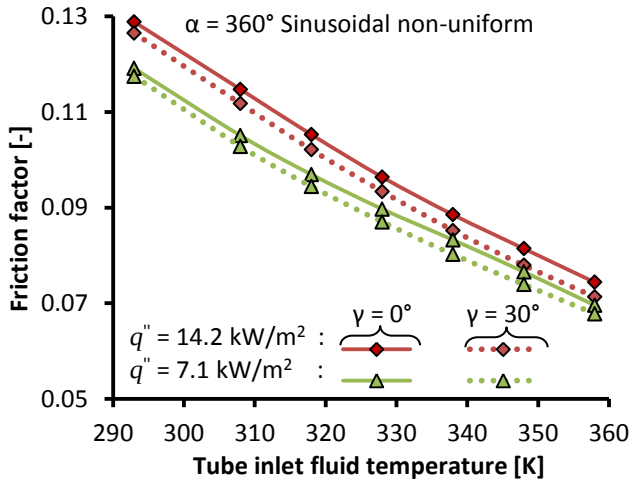

Figure 9 Variation of friction factor for inlet fluid temperature for symmetrical and asymmetrical non-uniform heat flux distribution

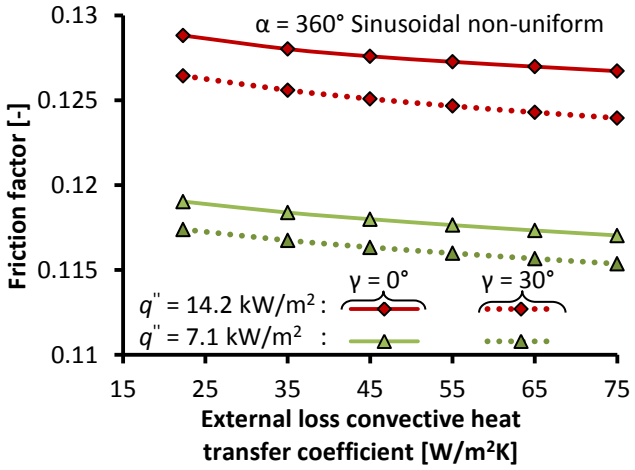

Figure 10 Influence of the external loss convective heat transfer coefficient on the friction factor

The friction factor for the case of 14.2 kW/m^2, where γ = 0° was 3.2 % higher than where γ = 30°, while for the case of 7.1 kW/m^2, it was 2.7 % higher where γ = 0° than where γ = 30° case. This indicates that friction factor of the tube model considered was influenced by the angle of inclination of the heat flux distribution boundary.

Figure 10 shows the influence of the external loss convective heat transfer coefficient on the friction factor for the heat flux distribution case in Figure 7. It was found that the friction factor for both the symmetrical (γ = 0°) and asymmetrical (γ = 30°) cases decreased with increase in the external loss convective heat transfer coefficient. It was also found that the friction factor decreased where γ = 30°. The friction factor for the case of 14.2 kW/m^2 where γ = 0° was 2% higher than where γ = 30°, while that for the case of 7.1 kW/m^2 where γ = 0° was 1.4% higher than where γ = 30°. This, however, shows that the effect of γ on the friction factor of the tube model considered was much higher for the fluid inlet temperature than for the external loss convective heat transfer coefficient.

CONCLUSION

Internal heat transfer coefficients and friction factors were obtained numerically for symmetrical and asymmetrical non-uniform heat flux cases in terms of the gravitational field. Results showed that the heat transfer coefficient for the non-uniform heat flux cases were higher than that of uniform heat flux cases, due to buoyancy effect. It was also found that the average heat transfer coefficient for symmetrical cases was higher than for asymmetrical cases. The heat transfer coefficient increased with the increase in the inlet fluid temperature and decreased with the increase in the external loss convective heat transfer coefficient. The friction factor for the uniform heat flux, symmetrical and asymmetrical non-uniform heat flux distributions decreased with the increase in the inlet fluid temperature and external loss convection heat transfer coefficient. The friction factors for the cases of symmetrical non-uniform heat flux distributions were higher than that of asymmetrical cases. This could be due to the decrease in buoyancy effect as the non-uniform heat flux distribution boundary deviates from the symmetrical axis of the tube.

REFERENCES

[1] Ghajar, A. J. and Tam, L.-M., Flow regime map for a horizontal pipe with uniform wall heat flux and three inlet configurations, Exp. Thermal and Fluid Sci. 10 (1995) 287-297.

[2] Barozzi, G. S., Zanchini, E. and Mariotti, M., Experimental investigation of combined forced and free convection in horizontal and inclined tubes, MECCANICA 20 (1985), 18-27

[3] Prayagi, S. V. and Thombre, S. B., Parametric studies on buoyancy induced flow through circular pipes in solar water heating system, International Journal of Engineering Science and Technology (IJEST) 3 (1) (2011) 616-627.

[4] Sadik K., Shah, R. K. and Aung W., *Handbook of Single-Phase Convective Heat Transfer*. A Wiley-Inter-Science Publication John Wiley & Sons New York, (1987).

[5] Touahri, S. and Boufendi T., Numerical study of the conjugate heat transfer in a horizontal pipe heated by Joulean effect, *Thermal Science*, Vol. 16 (1), Pp. 53-67, (2012).

[6] Zeitoun, O., Heat transfer for laminar flow in partially heated tubes, Alexandria Engineering Journal, Alexandria University, Egypt, 41 (2) (2002) 205-212.

[7] Okafor, I. F., Dirker, J. and Meyer, J. P., Numerical study of heat transfer characteristics for different solar flux distributions on linear Fresnel collector absorber tubes in laminar flow, Proceedings, IHTC 15-9221 August 10-15, 2014, Kyoto, Japan

[8] Okafor, I. F., Dirker, J. and Meyer, J. P., Influence of circumferential solar heat flux distribution on the heat transfer coefficients of linear Fresnel collector absorber tubes, Sol. Energy 107 (2014), 381-397.

[9] Cengel, Y. A. ,*Heat and Mass Transfer: A Practical Approach*, Third Edition. Published by McGraw-Hill Companies, Inc. 1221 Avenue of the Americas, New York, NY 10020, (2007).

[10] Duffie, J. A., Beckman, W. A., *Solar Engineering of Thermal Processes*, Second Edition, A Wiley-Interscience Publication, John Wiley & Sons, Inc. New York, (1980).

[11] Hameury, J., Hay, B., and Filtz, J- R., Measurement of total hemispherical emissivity using a calorimetric technique, Laboratoire National de Métrologie d'Essais (LNE), 29 Ave. Roger Hennequin, 78197 TRAPPES, France (2005) 1-14.

[12] ANSYS Fluent version 14.0, *Users' Guide ANSYS*, Release 14.0 Incorporated, Southpointe 275 Technology Drive Canonsburg, PA 15317, (2011).

[13] Reddy, K. S., Sendhil, K., An improved model for natural convection heat loss from modified cavity receiver of solar dish concentrator, *Solar Energy*, 83, pp. 1884 –1892, (2009).

[14] Patankar, S.V., *Numerical Heat Transfer and Fluid Flow*, Hemisphere Publishing Corporation, USA, (1980).